npj | climate and atmospheric science

Article

Published in partnership with CECCR at King Abdulaziz University

https://doi.org/10.1038/s41612-025-00948-7

Moderate climate sensitivity due to opposing mixed-phase cloud feedbacks

Ivy Tan[1] ✉, Chen Zhou[2], Aubert Lamy[1] & Catherine L. Stauffer[1]

Earth's climate sensitivity quantifies the ultimate change in global mean surface air temperature in response to a doubling of atmospheric CO_2 concentrations. Recent assessments estimate that Earth's climate sensitivity *very likely* lies between 2.3 °C and 4.7 °C, with the representation of clouds in climate models accounting for a large portion of its uncertainty. Here, we adjust the climate sensitivity of individual contemporary climate models after using satellite observations to alleviate biases in their representation of mixed-phase clouds. A resulting moderate average climate sensitivity of 3.63 ± 0.98(1σ) °C arises due to opposing responses of clouds. While increasing the proportion of liquid within cold clouds prior to CO_2 doubling increases climate sensitivity via transitions from solid to liquid hydrometeors, a strongly opposing increase in reflective cloud cover decreases climate sensitivity. This emphasizes the need to reconsider the role of mixed-phase cloud cover changes in climate sensitivity assessments.

How much will Earth ultimately warm in response to a doubling of atmospheric CO_2 concentrations? The answer to this fundamental question about the *climate sensitivity* of Earth has plagued climate science for decades. Early estimates of Earth's climate sensitivity spanned 3 °C, ranging from 1.5 °C to 4.5 °C[1]. Global climate models (GCMs) participating in the Fifth Phase of the Coupled Model Intercomparison Project (CMIP5) have since estimated a narrower range spanning from 2.0 °C to 4.6 °C[2]. However, the range in climate sensitivity estimated by GCMs participating in the most recent Sixth Phase of the Coupled Model Intercomparison Project (CMIP6) has increased by 1.2 °C relative to CMIP5 and now spans from 1.8 °C to 5.6 °C[3]. Moreover, of the GCMs participating in CMIP6, 9 out of 27 of them estimate a climate sensitivity value that exceeds the upper range of 4.6 °C estimated by the GCMs participating in CMIP5. This "hot model problem"[4] has since been reconciled with expert judgment based on data from the historical period and paleoclimate records resulting in a *very likely* (5–95%) range of 2.3 °C to 4.7 °C[5]. This range is comparable to but 0.6 °C narrower than the *very likely* range of 2 °C to 5 °C derived in the IPCC's most recent Sixth Assessment Report[6].

The representation of the surface temperature-mediated response of clouds in GCMs is a longstanding and dominant source of uncertainty in climate sensitivity[6,7]. Many studies have since focused on identifying sources of errors in the representation of clouds in GCMs that impact climate sensitivity in various latitudinal regions[8–13]. In the extratropical regions, transitions in the thermodynamic phase of hydrometeors within mixed-phase clouds in the ~−38 °C to 0 °C temperature range are a robust feature of global warming experiments performed by GCMs[14]. This *cloud-phase feedback* involves the replacement of ice with supercooled liquid within mixed-phase clouds due to the deepening of the troposphere in response to global warming[15]. Since liquid droplets are typically more abundant and smaller in size compared to ice crystals[16], the transition to more liquid-dominated mixed-phase clouds in response to global warming reflects more sunlight back out to space[17]. The net result is a negative feedback that counteracts global warming, with pre-warmed climate states exhibiting lower supercooled liquid fractions within mixed-phase clouds leading to a more negative feedback due to the larger replacement of ice with liquid due to the cloud-phase feedback. Many of the GCMs participating in CMIP5 were found to underestimate the supercooled liquid fraction within mixed-phase clouds relative to satellite observations on a global scale[18,19]. When the supercooled liquid fractions of these GCMs were composited in temperature bins over the Southern Ocean, the temperature at which half of the clouds glaciated—termed *T50*—exhibited a spread of nearly 40 °C, with the majority of GCMs producing excessively warm T50 values that indicate an underestimate in the supercooled liquid fraction within mixed-phase clouds[20].

Results

Evolution of cloud phase partitioning from CMIP5 to CMIP6

Several GCMs participating in CMIP6 have since improved their representation of mixed-phase clouds[21–23]. To examine how T50 evolved from CMIP5 and CMIP6, we systematically calculate T50 for the full ensemble of 61 GCMs with available data from experiments representative of pre-industrial conditions (piControl)[24,25]. These calculations use cloud mixing ratios and local temperature in model grid cells. We focused on the extratropics (latitudes poleward of 60° in both hemispheres) as mixed-phase

[1]McGill University, Montreal, QC, Canada. [2]Nanjing University, School of Atmospheric Sciences, Nanjing, China. ✉e-mail: ivy.tan@mcgill.ca

clouds are particularly ubiquitous in these regions[26–31]. We also calculate T50 produced by experiments holding sea surface temperature and sea ice constant to 1978 – 2006 conditions (AMIP)[32]. We additionally calculated T50 using occurrences of cloud liquid and ice produced by a lidar simulator designed to be consistent with an active satellite product, GCM-Oriented CALIPSO Cloud Product (GOCCP)[33] derived from the Cloud-Aerosol Lidar with Orthogonal Polarization (CALIOP) instrument[34] within the Cloud Feedback Model Intercomparison Project (CFMIP) Observation Simulator Package (COSP) framework[35].

Overall, the ensemble mean T50 of the GCMs participating in CMIP6 is −21 °C and is 4.2 °C colder than the ensemble mean T50 of —15.8 °C of the GCMs participating in CMIP5 (Fig. 1). Observations of T50 derived from GOCCP yield a T50 estimate of −19.7 °C in the extratropics. This observed T50 value is comparable to the multimodel ensemble average of −21 °C in CMIP6, however, arises from averaging 18 GCMs that overestimate the fraction of supercooled liquid water within mixed-phase clouds and 17 GCMs that underestimate this fraction. This contrasts with the 21 out of 26 GCMs that underestimate the supercooled liquid fraction of mixed-phase clouds in participating in CMIP5. The spread in T50 in both generations of GCMs is equally large, spanning ≈30 °C.

The generally enhanced proportion of supercooled liquid water within mixed-phase clouds simulated by the most recent generation of GCMs participating in CMIP6 (Fig. 1) is consistent with previous literature[21,22,36,37]; there are more GCMs with cold T50 values in CMIP6 than CMIP5, and several GCMs simulate T50 values close to the homogeneous freezing temperature of ≈−38 °C. This result is consistent across both piControl and AMIP experiments as most GCMs produce similar T50 values for both experiments (Fig. S1a). However, the COSP lidar simulator produces a dissimilar distribution of T50 values, with values that are ≥9 °C colder than those calculated using the raw cloud mass variables in half of the GCMs with data available (Fig. S1b). Indeed, a recent reexamination of the thresholds of layer-integrated depolarization ratio and layer-integrated attenuated backscatter of fully attenuating clouds that are incorporated in the CALIOP phase discrimination algorithm suggests a greater proportion of ice hydrometeors within mixed-phase clouds than originally reported[38]. For example, equatorward of 50°S in the Southern Ocean where mixed-phase clouds are ubiquitous, a T50 value of ≈ −26 °C was derived from the vantage point of ship-based lidar observations while the T50 value based on spaceborne lidar observations shows substantially more liquid and is ≈−31 °C[39]. Therefore, the lidar simulator potentially overestimates the fraction of supercooled liquid within mixed-phase clouds and we use the raw GCM cloud mass variables in our main analysis to maximize the number of GCMs in our analysis.

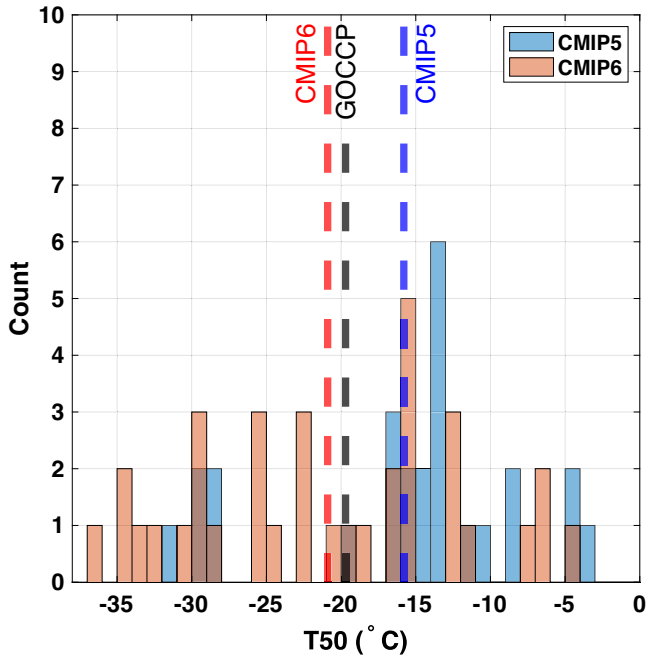

Fig. 1 | Histogram quantifying the evolution of T50 from CMIP5 to CMIP6. Counts represent the number of GCMs participating in CMIP5 (blue) and CMIP6 (orange) with extratropical T50 values within a 1 °C bin. The red, black, and blue dashed lines represent the average T50 across all GCMs participating in CMIP6, the observed T50 derived from GOCCP, and the average T50 across all GCMs participating in CMIP5, respectively.

Cloud phase and cloud feedback relationships in GCMs

A negative linear relationship between T50 in the pre-warmed climate state and the shortwave (SW) cloud optical depth feedback (λ_τ) in response to global warming was demonstrated in an ensemble of perturbed cloud microphysics experiments in two GCMs[40,41]. The linear relationship was particularly prominent in the extratropics and was linked to the cloud-phase feedback. Given the greater proportion of mixed-phase cloud liquid mass in the piControl simulations in CMIP6 (Fig. 1), we examine whether the relationship between T50 and the SW λ_τ previously simulated by the ensemble of perturbed microphysics experiments extends to the full ensemble of GCMs participating in CMIP5 and CMIP6.

A negative linear correlation between T50 and the SW λ_τ in the extratropics emerges in 61 GCMs participating in CMIP5 and CMIP6 (Fig. 2a). This negative correlation is consistent with the cloud-phase feedback: GCMs with warmer T50 values contain relatively higher proportions of ice within mixed-phase clouds that become replaced with optically thicker and thus more reflective liquid droplets in response to global warming that in turn induce a more negative λ_τ. The negative relationship is stronger in CMIP5 than in CMIP6 (Fig. S2a, S2b). However, at the same time, a competing positive linear relationship between T50 and changes in cloud amount in response to a quadrupling of CO_2, i.e. the SW cloud amount feedback (λ_{amt}) also emerges (Fig. 2b). This positive linear relationship is also stronger among the GCMs participating in CMIP5 (Fig. S2c) compared to the GCMs participating in CMIP6 (Fig. S2d) and has recently been attributed to a "supercooled cloud feedback"[37]. In this feedback, the supercooled liquid within clouds shift to warm liquid water clouds at temperatures above freezing in response to global warming. Since supercooled liquid water-containing clouds precipitate more efficiently than warm liquid water-containing clouds[42–44], transitions from the former to the latter in response to global warming would result in increases in the coverage of reflective clouds and therefore a negative SW λ_{amt}. As such, T50 is positively correlated with λ_{amt}. This supercooled cloud feedback associated with λ_{amt} dominates the "cloud lifetime feedback"[45,46] that would otherwise result in a negative relationship between T50 and λ_{amt}. This latter cloud lifetime feedback is associated with the extended longevity of mixed-phase clouds that are composed of larger amounts of cloud liquid due to the lower precipitation efficiency of liquid droplets compared to ice crystals.

Adjustment of climate sensitivity via mixed-phase clouds

Given the linear T50-λ_τ and T50-λ_{amt} relationships (Fig. 2), we now exploit these relationships to adjust the climate sensitivity of each individual GCM based on its bias in T50 relative to GOCCP observations. Our method is based on the forcing-feedback framework[47], where the change in the net global mean radiative flux at the top of the atmosphere in response to radiative forcing, ΔN, can be expressed as

$$\Delta N = F + \lambda \Delta T_s, \quad (1)$$

where F is the global mean radiative forcing perturbation, λ is the climate radiative feedback parameter in response to F, and ΔT_s is the change in global mean surface air temperature in response to F. λ can be decomposed into the summation of surface and air temperature feedbacks, the albedo feedback, the water vapor feedback, and the cloud feedback, each of which can be further decomposed into the sum of their SW and longwave contributions[48]. The cloud feedback can also be decomposed into a sum of

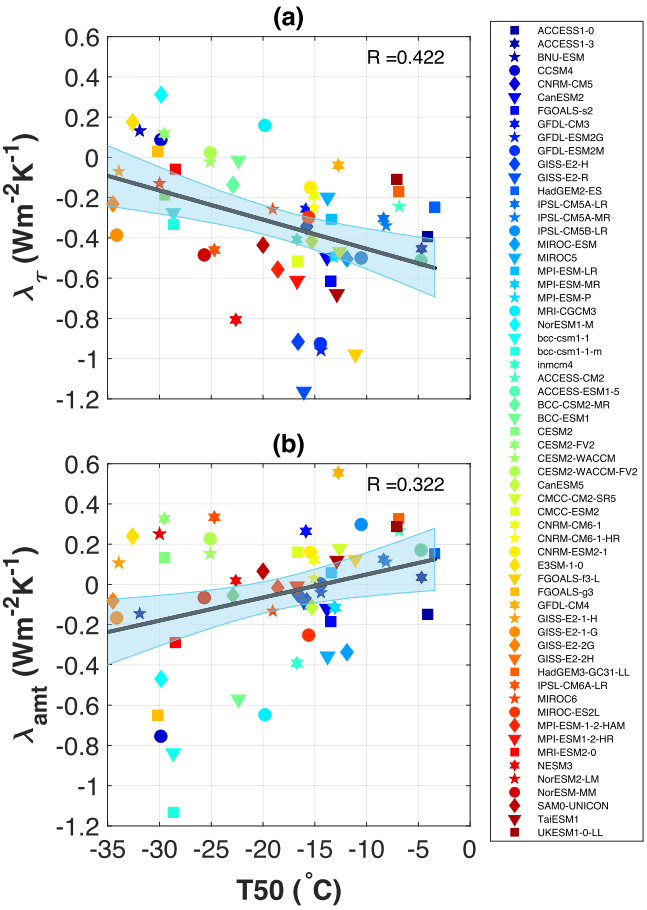

Fig. 2 | Relationship between extratropical T50 and SW extratropical cloud feedbacks in GCMs participating in CMIP5 and CMIP6. Linear relationship between (**a**) λ_τ and T50 and (**b**) λ_{amt} and T50. Each data point represents a GCM labeled in the legend. The least squares regression slope is displayed as the solid black line and the 95% confidence interval of the predicted value of the linear regression model is shaded in blue. The correlation coefficient is displayed in the top-right corner in each panel.

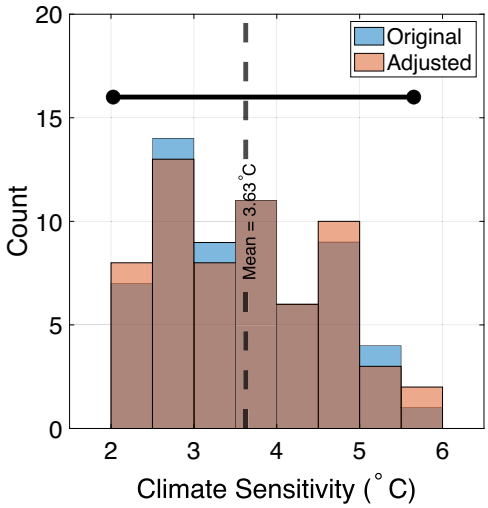

Fig. 3 | Histogram of the climate sensitivity of GCMs and their climate sensitivity values after adjusting for biases in the partitioning of cloud thermodynamic phase in mixed-phase clouds in GCMs. The original climate sensitivity values are displayed in blue and adjusted climate sensitivity values are displayed in red. The black dashed line represents the mean of the original and adjusted ECS values, which are approximately equal. The black horizontal line represents the range in climate sensitivity derived using the 95% confidence intervals of the linear regressions in Fig. 2.

contributions from cloud property changes including the SW λ_τ and λ_{amt} feedbacks that both exhibit a linear relationship with T50 (Fig. 2). However, T50 is a biased estimator of the observed T50 (Fig. 1). The bias of the extratropical T50 for every GCM can be calculated as

$$\Delta T50_i = T50_i - T50_o, \tag{2}$$

where $T50_o$ is the observed extratropical T50 derived from GOCCP and the subscript i denotes an individual GCM. For CMIP5 and CMIP6, we analyzed 26 and 35 GCMs, respectively. Through the linear T50-λ_τ and T50-λ_{amt} relationships established in the GCMs participating in CMIP5 and CMIP6, the biases in λ_τ and λ_{amt} can correspondingly be calculated as

$$\Delta\lambda_{c,i} = m \cdot \Delta T50_i, \tag{3}$$

where the subscript c represents either τ or amt, and m represents the slope of the least squares regression fit in Fig. 2. Substituting Eq. (3) back into Eq. (1), and solving for ΔT_s while assuming a vanishing value of ΔN at equilibrium yields the climate sensitivity of each individual GCM after adjusting for biases in T50,

$$ECS_{adj,i} = -\frac{F_i}{\lambda_i - w\left(\Delta\lambda_{\tau,i} + \Delta\lambda_{amt,i}\right)} \tag{4}$$

where $w \approx 0.15$ represents the areal fraction of the extratropics to that of the entire globe. F and λ were calculated as half the value of the y-intercept and the slope, respectively, of the least squares linear regression of the global annual mean change in the net radiative flux at the top of the atmosphere against the change in global annual mean surface temperature for 150 years of the piControl and abrupt4xCO2 experiments[47]. Our method assumes that all other feedbacks in the climate system are held constant in the adjustment process. This contrasts with other methods that have observationally constrained T50 by way of modifying the representations of cloud physical processes within a given model that in turn interacted with other model processes[40,41,49].

The average climate sensitivity after adjusting for cloud feedback biases via their relationship with T50 based on 61 GCMs participating in both CMIP5 and CMIP6 is 3.63 K (Fig. 3). This value results from a downward adjustment of climate sensitivity from 3.28 K to 3.24 K based on the GCMs participating in CMIP5 (Fig. S3a) and essentially no change in the climate sensitivity of 3.86 K based on the GCMs participating in CMIP6 (Fig. S3b). In CMIP5, the downward adjustment in climate sensitivity results from upward adjustments via λ_τ (Fig. S3c) being overwhelmed by downward adjustments via λ_{amt} (Fig. S3e) while negligible adjustments in climate sensitivity occur due to λ_τ (Fig. S3e) and λ_{amt} in CMIP6 (Fig. S3f). Since the majority of the GCMs participating in CMIP5 underestimate the supercooled liquid fraction within mixed-phase clouds relative to the observations (Fig. 1) such that ΔT50 is positive for these GCMs, $ECS_{adj,i}$ in Eq. (4) for these GCMs is therefore adjusted to larger values from the adjustment of λ_i to more positive values via $\lambda_{\tau,i}$. The upward adjustment of the climate sensitivity of the GCMs participating in CMIP5 due to the λ_τ alone, i.e. assuming a vanishing value of λ_{amt}, is consistent with previous studies of the influence of T50 on the cloud-phase feedback[15,40]. However, due to the steeper slope in the T50-λ_{amt} relationship of the opposite sign, $ECS_{adj,i}$ of these same GCMs will be adjusted to small values.

In contrast, the lack of change in climate sensitivity in the GCMs participating in CMIP6 results from adjustments that are approximately canceled due to the equal number of GCMs that overestimate and underestimate the supercooled liquid fraction within mixed-phase clouds relative to observations. In contrast to the 26 GCMs participating in CMIP5, of the 35 GCMs considered (Fig. S4a), λ_τ was adjusted downward for approximately half of the GCMs while λ_τ was adjusted upward for the other half of

the GCMs (Fig. S4b). The approximately equal number of GCMs that overestimate and underestimate T50 relative to observations results in a near-zero adjustment in the mean climate sensitivity from their original values via biases in λ_τ. Conversely, λ_{amt} was correspondingly adjusted upward for the GCMs that produced λ_τ values that were adjusted downward while λ_{amt} was correspondingly adjusted downward for the GCMs that produced λ_τ values that were adjusted upward. This similarly also resulted in a near-zero adjustment in the mean climate sensitivity from their original values via biases in λ_{amt}. We also note that despite the fact that we chose to analyze raw model cloud mass instead of COSP lidar simulator data to maximize the number of GCMs in our analysis, the fact that λ_τ and λ_{amt} have opposing effects on climate sensitivity ultimately leads to negligible material difference in our adjusted climate sensitivity estimate.

Discussion

The average adjusted climate sensitivity of 3.63 °C arising from corrections to biases in the thermodynamic phase partitioning within the mixed-phase clouds in GCMs participating in CMIP5 and CMIP6 suggests a moderate climate sensitivity that is within the *very likely* range based on two different assessments[5,6]. Our estimate is also in line with recent estimates of 3.56 ±0.72 K and 3.47 ±0.33 K derived from observational constraints on low-level clouds equatorward of 60° in both hemispheres[11] and those confined to the subtropics[12], respectively. Our results thus provide additional support for a moderate climate sensitivity based on complementary observational constraints on extratropical mixed-phase clouds in a total of 61 GCMs. While seemingly contradictory to previous literature showing a rise in climate sensitivity in GCMs when mixed-phase clouds are constrained by observations, the rise in climate sensitivity due to the cloud-phase feedback is consistent; rather, it is the role of λ_{amt} that unexpectedly emerges in GCMs causing a decrease in the average climate sensitivity in CMIP5. Namely, the positive relationship between T50 and λ_{amt} hypothesized to be due to the supercooled cloud feedback[37] strongly opposes and dominates the negative relationship between T50 and λ_τ in CMIP5. This positive relationship between T50 and λ_{amt} albeit with a weaker magnitude was shown to exist in a single GCM (Fig. S2[40]); however, is opposite in sign to the response attributed to entrainment of dry air into the boundary layer as a result of increasing the mixed-phase supercooled liquid fraction achieved by perturbing the GCM's shallow convective detrainment scheme[49]. This suggests that the response of λ_{amt} to perturbations in T50 is sensitive to physical parameterizations in GCMs.

Our findings highlight the need to consider changes in the horizontal coverage of clouds in addition to their changes in opacity in response to global warming as they can have a strong opposing effect on climate sensitivity in some GCMs depending on their treatment of cloud physical processes.

Methods

Calculation of T50

The mass fraction of cloud water ('clw') and the mass fraction of cloud ice ('cli') were first vertically interpolated to the 17 and 19 standard pressure levels of CMIP5 and CMIP6, respectively. The ratio of 'clw' to the sum of 'clw' and 'cli' was then calculated and composited in 1 °C air temperature bins for grid cells at latitudes poleward of 60°. T50 was calculated as the median air temperature at which 0.48 'clcalipsoliq' and 'clcalipsoice' in AMIP experiments in place of 'clw' and 'cli', respectively, however, these variables were only available for a limited number of GCMs participating in CMIP6. Since 'clcalipsoliq' and 'clcalipsoice' are provided in height coordinates, air temperature was instead vertically interpolated to height coordinates before calculating the ratio of 'clcalipsoliq' to the sum of 'clcalipsoliq' and 'clcalipsoice' and compositing this quantity in 1 °C air temperature bins for all grid cells at latitudes poleward of 60°.

The observed T50 value was also calculated following the same method using the frequency of liquid and ice cloud occurrences and the air temperature at the corresponding locations at 3 °C resolution that are provided by the GOCCP product. Both daytime and nighttime observations were used and the calculations were performed for the time period from 2007-2019, excluding 2016 due to missing data.

Calculation of λ_τ and λ_{amt}

The SW λ_τ and SW λ_{amt} values were calculated using the approximate partial radiative perturbation (APRP) method[50] applied to the piControl and abrupt4xCO2 experiments. This method is a simplified version of the partial radiative perturbation method[51]. This simplified model assumes that the atmosphere is a single layer that scatters and absorbs radiation, but that incident radiation is only absorbed in its first transit through the layer. SW cloud feedbacks are obtained from the APRP method by first calculating the planetary albedo as a function of seven parameters detailed in ref. 50 that are based on the following variables: the cloud area fraction (including stratiform and convective clouds) defined for the whole atmospheric column, as seen from the surface or the top of the atmosphere (CMIP variable "clt"), incident SW radiative flux at the top of the atmosphere (CMIP variable "rsdt"), outgoing SW radiative flux at the top of the atmosphere (CMIP variable "rsut"), outgoing clear-sky SW radiative flux at the top of the atmosphere (CMIP variable "rsutcs"), downwelling SW radiative flux (CMIP variable "rsds"), downwelling clear-sky SW radiative flux (CMIP variable "rsdscs"), upwelling SW radiative flux (CMIP variable "rsus"), and upwelling clear-sky SW radiative flux (CMIP variable "rsuscs"). Akin to the PRP method, the process of calculating a feedback parameter with the APRP method involves running an offline radiative transfer model to calculate the change in radiative fluxes when the variable associated with the feedback parameter of interest from the perturbed climate state is substituted into the control climate state. For example, changes in cloud amount, C, in a control climate (state 1) due to a quadrupling of CO_2 (state 2) would result in a cloud amount radiative feedback that would be calculated as $R(C_2, x1, y1, \ldots) - R(C_1, x1, y1, \ldots)$ normalized by the change in surface air temperature, where x and y are other state variables on which the radiative fluxes, R depend.

To be consistent with previous studies, we take λ_τ to be the summation of the SW scattering and absorption feedbacks[3] for clouds at all vertical levels. λ_{amt} represents the change in cloud amount at all vertical levels due to an abrupt quadrupling of atmospheric carbon dioxide concentrations. Monthly anomalies of the extratropical cloud-induced SW radiative fluxes at the top of the atmosphere were linearly regressed against monthly anomalies of global mean surface air temperature to calculate SW λ_τ and SW λ_{amt}. The SW scattering feedback is calculated as the sum of the average values of a "forward calculation" and a "backward calculation" linearly regressed onto global mean surface air temperature anomalies. The "forward calculation" is the difference between the planetary albedo calculated with the scattering coefficient from the abrupt4xCO2 experiment and the planetary albedo calculated with all other fields in the piControl state. The "backward calculation" is the difference between the planetary albedo calculated with the scattering coefficient from the piControl experiment and the planetary albedo calculated with all other fields in the abrupt4xCO2 state. The absorption feedback and λ_{amt} are similarly calculated except with the absorption coefficient and cloud area fraction ("clt"), respectively, in place of the scattering coefficient. The reader is referred to Taylor et al.[50] for details.

Quantifying uncertainty

The 95% confidence interval of the slope of the linear regression was used to resample the slope 2000 times using a bootstrapping method. This produces a distribution of 2000 additional $\Delta\lambda_\tau$ values following Eq. (3). The same procedure was repeated for the slope of the T50-λ_{amt} relationship to obtain a distribution of 2000 additional $\Delta\lambda_{amt}$ values following Eq. (3). These $\Delta\lambda_\tau$ and $\Delta\lambda_{amt}$ were then inserted into Eq. (4) to calculate a distribution of 2000 additional adjusted climate sensitivity values. The maximum and minimum of these 2000 additional adjusted climate sensitivity values were taken to represent the 5 to 95% confidence interval in Fig. 3.

Data availability

The data analyzed in this study is freely available via ESGF: https://aims2.llnl.gov/.

Received: 1 October 2024; Accepted: 11 February 2025;
Published online: 04 March 2025

References

1. Council, N. R. *Carbon dioxide and climate: a scientific assessment* (National Academy of Sciences, Washington, DC, 1979).
2. Mauritsen, T. & Stevens, B. Missing iris effect as a possible cause of muted hydrological change and high climate sensitivity in models. *Nat. Geosci.* **85** (2015).
3. Zelinka, M. D. et al. Causes of higher climate sensitivity in CMIP6 models. *Geophys. Res. Lett.* **47**, e2019GL085782 (2020).
4. Hausfather, Z., Marvel, K., Schmidt, G. A., Nielsen-Gammon, J. W. & Zelinka, M. Climate simulations: recognize the 'hot model' problem. *Nature* **605**, 26–29 (2022).
5. Sherwood, S. C. et al. An assessment of Earth's climate sensitivity using multiple lines of evidence. *Rev. Geophys.* **58**, e2019RG000678 (2020).
6. Forster, P. et al. *The Earth's Energy Budget, Climate Feedbacks, and Climate Sensitivity. In Climate Change 2021: The Physical Science Basis. Contribution of Working Group I to the Sixth Assessment Report of the Intergovernmental Panel on Climate Change* (Cambridge University Press, 2021).
7. Cess, R. D. et al. Interpretation of cloud-climate feedback as produced by 14 atmospheric general circulation models. *Science* **245**, 513–516 (1990).
8. Bony, S. & Dufresne, J.-L. Marine boundary layer clouds at the heart of tropical cloud feedback uncertainties in climate models. *Geophys. Res. Lett.* **32**, L20806 (2005).
9. Terai, C. R., Klein, S. A. & Zelinka, M. D. Constraining the low-cloud optical depth feedback at middle and high latitudes using satellite observations. *J. Geophys. Res.* **121**, 9696–9716 (2016).
10. Lipat, B. R., Tselioudis, G., Grise, K. M. & Polvani, L. M. CMIP5 models' shortwave cloud radiative response and climate sensitivity linked to the climatological Hadley cell extent. *Geophys. Res. Lett.* **44**, 5739–5748 (2017).
11. Myers, T. A. et al. Observational constraints on low cloud feedback reduce uncertainty of climate sensitivity. *Nat. Clim. Change* **11**, 501–507 (2021).
12. Cesana, G. & Genio, A. D. D. Observational constraint on cloud feedbacks suggests moderate climate sensitivity. *Nat. Clim. Change* **11**, 213–218 (2021).
13. McCoy, D. T. et al. Extratropical shortwave cloud feedbacks in the context of the global circulation and hydrological cycle. *Geophys. Res. Lett.* **49**, e2021GL097154 (2022).
14. Tsushima, Y. et al. Importance of the mixed-phase cloud distribution in the control climate for assessing the response of clouds to carbon dioxide increase: a multi-model study. *Clim. Dyn.* **27**, 113–126 (2006).
15. Mitchell, J. F. B., Senior, C. A. & Ingram, W. J. CO_2 and climate: a missing feedback? *Nature* **341**, 132–134 (1989).
16. Pruppacher, H. R. & Klett, J. D. *Microphysics of Clouds and Precipitation* Vol. 18 (Springer, 2010).
17. Sun, Z. & Shine, K. P. Studies of the radiative properties of ice and mixed-phase clouds. *Q. J. R. Meteorol. Soc.* **120**, 111–137 (1994).
18. Komurcu, K. et al. Intercomparison of the cloud water phase among global climate models. *J. Geophys. Res.* **119**, 3372–3400 (2014).
19. Cesana, G., Waliser, D. E., Jiang, X. & Li, J. L. F. Multimodel evaluation of cloud phase transition using satellite and reanalysis data. *J. Geophys. Res.* **120**, 7871–7892 (2015).
20. McCoy, D. T., Tan, I., Hartmann, D. L., Zelinka, M. D. & Storelvmo, T. On the relationships among cloud cover, mixed-phase partitioning, and planetary albedo in GCMS. *J. Adv. Model. Earth Syst.* **8**, 650–668 (2016).
21. Bodas-Salcedo, A. et al. Strong dependence of atmospheric feedbacks on mixed-phase microphysics and aerosol-cloud interactions in HadGEM3. *J. Adv. Mod. Earth Syst.* **11**, 1735–1758 (2019).
22. Kawai, H. et al. Significant improvement of cloud representation in the global climate model MRI-ESM2. *Geosci. Mod. Dev.* **12**, 2875–2897 (2019).
23. Zhang, Y. et al. Understanding changes in cloud simulations from E3SM version 1 to version 2. *Geosci. Model Dev.* **17**, 169–189 (2024).
24. Taylor, K. E., Stouffer, R. J. & Meehl, G. A. An overview of CMIP5 and the experiment design. *Bull. Am. Meteorol. Soc.* **93**, 485–498 (2012).
25. Eyring, V. et al. Overview of the Coupled Model Intercomparison Project Phase 6 (CMIP6) experimental design and organization. *Geosci. Mod. Dev.* **9**, 1937–1958 (2016).
26. Shupe, M. D., Matrosov, S. Y. & Uttal, T. Arctic mixed-phase cloud properties derived from surface-based sensors at SHEBA. *J. Atmos. Sci.* **63**, 697–711 (2006).
27. Hu, Y. et al. Occurrence, liquid water content, and fraction of supercooled water clouds from combined CALIOP/IIR/MODIS measurements. *J. Geophys. Res*. **115** (2010).
28. Huang, Y., Siems, S. T., Manton, M. J., Protat, A. & Delanoe, J. A study on the low-altitude clouds over the Southern Ocean using the DARDAR-MASK. *J. Geophys. Res*. **117** (2012).
29. Mioche, G., Jourdan, O., Ceccaldi, M. & Delanoe, J. Variability of mixed-phase clouds in the Arctic with a focus on the Svalbard region: a study based on spaceborne active remote sensing. *Atmos. Chem. Phys.* **15**, 2445–2461 (2015).
30. Zhang, D. et al. Comparison of antarctic and arctic single-layer stratiform mixed-phase cloud properties using ground-based remote sensing measurements. *J. Geophys. Res.* **124**, 10186–10204 (2019).
31. Tan, I., Storelvmo, T. & Yong-Sang Choi, Y.-S. Spaceborne lidar observations of the ice-nucleating potential of dust, polluted dust, and smoke aerosols in mixed-phase clouds. JGR Atmos. https://doi.org/10.1002/2013JD021333 (2014).
32. Gates, W. L. AMIP: The Atmospheric Model Intercomparison Project. *Bull. Am. Meteorol. Soc.* **73**, 1962–1970 (1992).
33. Chepfer, H. et al. The GCM-oriented calipso cloud product (CALIPSO-GOCCP). *J. Geophys. Res*. **115** (2010).
34. Winker, D. et al. The CALIPSO mission. *Bull. Am. Meteorol. Soc.* **91**, 1211–1230 (2010).
35. Bodas-Salcedo, A. et al. COSP: Satellite simulation software for model assessment. *Bull. Am. Meteorol. Soc.* **92**, 1023–1043 (2011).
36. Zhang, M. et al. Cloud phase simulation at high latitudes in EAMv2: Evaluation using CALIPSO observations and comparison with EAMv1. *J. Geophys. Res.* **127**, e2022JD037100 (2022).
37. Cesana, G. et al. Observational constraint on a feedback from supercooled clouds reduces projected warming uncertainty. *Commun. Earth Environ.* **5** (2024).
38. Mace, G. G., Benson, S. & Hu, Y. On the frequency of occurrence of the ice phase in supercooled Southern Ocean low clouds derived from CALIPSO and CloudSat. *Geophys. Res. Lett.* **47**, e2020GL087554 (2020).
39. Mace, G. G., Protat, A. & Benson, S. Mixed-phase clouds over the southern ocean as observed from satellite and surface based lidar and radar. *J. Geophys. Res.* **126**, e2021JD034569 (2021).
40. Tan, I., Storelvmo, T. & Zelinka, M. D. Observational constraints on mixed-phase clouds imply higher climate sensitivity. *Science* **352**, 224–227 (2016).
41. Tan, I., Barahona, D. & Coopman, Q. Potential link between ice nucleation and climate model spread in Arctic amplification. *Geophys. Res. Lett.* **49**, e2021GL097373 (2022).
42. Senior, C. A. & Mitchell, J. F. B. Carbon dioxide and climate. *J. Clim.* **6**, 393–418 (1993).
43. Hoose, C., Lohmann, U., Bennartz, R., Croft, B. & Lesins, G. Global simulations of aerosol processing in clouds. *Atmos. Chem. Phys.* **8**, 6939–6963 (2008).
44. Stanford, M. W. et al. Earth-system-model evaluation of cloud and precipitation occurrence for supercooled and warm clouds over the

Southern Ocean's Macquarie Island. *Atmos. Chem. Phys.* **23**, 9037–9069 (2023).
45. Tan, I. & Storelvmo, T. Evidence of strong contributions from mixed-phase clouds to arctic climate change. *Geophys. Res. Lett.* **46**, 2894–2902 (2019).
46. Mulmenstadt, J. et al. An underestimated negative cloud feedback from cloud lifetime changes. *Nat. Clim. Change* **11**, 508–513 (2021).
47. Gregory, J. M. et al. A new method for diagnosing radiative forcing and climate sensitivity. *Geophys. Res. Lett*. **31** (2004).
48. Soden, B. J., Held, I. M. & Colman, R. Quantifying climate feedbacks using radiative kernels. *J. Clim.* **21**, 3504–3520 (2008).
49. Frey, W. R. & Kay, J. E. The influence of extratropical cloud phase and amount feedbacks on climate sensitivity. *Clim. Dyn.* **50**, 3097–3115 (2018).
50. Taylor, K. E. et al. Estimating shortwave radiative forcing and response in climate models. *J. Clim.* **20**, 2530–2543 (2007).
51. Wetherald, R. T. & Manabe, S. Cloud feedback processes in a general circulation model. *J. Atmos. Sci*. **45** (1988).

Acknowledgements

This research was supported by the Natural Sciences and Engineering Research Council of Canada (NSERC), RGPIN-2021-02720 and enabled in part by support provided by the Digital Research Alliance of Canada.

Author contributions

I.T. prepared all figures and wrote the manuscript. I.T. and C.Z. conceived the methods. A.L. and C.S. contributed to the analysis. All authors reviewed the manuscript.

Competing interests

The authors declare no competing interests.

Additional information

Supplementary information The online version contains supplementary material available at https://doi.org/10.1038/s41612-025-00948-7.

Correspondence and requests for materials should be addressed to Ivy Tan.